DOI: 10.37190/abb/205428

# Blood flow simulations in a cerebral aneurysm secured by a Flow Diverter stent

Zbigniew Tyfa[1], Karol Wiśniewski[1,2], Piotr Reorowicz[1], Krzysztof Jóźwik[1]

[1]Institute of Turbomachinery, Lodz University of Technology, Lodz, Poland
[2]Department of Neurosurgery and Neurooncology, Medical University of Lodz, Barlicki University Hospital, Lodz, Poland
*Corresponding author: Zbigniew Tyfa, Institute of Turbomachinery, Lodz University of Technology, Lodz, Poland, e – mail address: zbigniew.tyfa@p.lodz.pl



Submitted: 21st February 2025

Accepted: 21st May 2025

## Abstract

**Objective:** The objective of this research was to show a potential use of computational fluid dynamics tools in supporting the medical personnel by offering objective data regarding the hemodynamic changes in the aneurysm caused by implanting different models of the stent.

**Methods:** The authors reconstructed patient-specific model of the cerebral arteries with diagnosed aneurysm. Then, four virtual models of the Flow Diverter stent (with varied nominal diameters) were prepared. During the numerical analyses, the Immersed Solid Method was used to model the presence of the stent wirebraid. After performing steady state and transient simulations of non-Newtonian blood flow in pre- and post-treatment models, changes in numerous hemodynamic parameters were analysed.

**Results:** The results confirmed that stent porosity influences hemodynamic changes inside the aneurysm (for presented case studies). The less porous the stent, the more it promotes the possible intrasaccular thrombosis. This could be concluded by observing larger regions of stagnant blood with higher viscosity. Additionally, the denser the stent, the lower and more uniform the stress exerted on the aneurysm wall.

**Conclusions:** Numerical simulations can provide valuable insight into phenomena occurring inside the blood flow after implanting the stent. This can support selecting optimal stent configuration for the particular patient and, consequently, can help in planning the endovascular procedure.

**Keywords**: intracranial aneurysm, CFD, Flow Diverter stent, blood flow simulations



## 1. Introduction

In middle-income European countries, cardiovascular diseases (CDs) constitute in 36% of the mortality rate both for females and males. In high-income countries these values are equal to 16% and 24% for females and males, respectively [29]. One of CDs are aneurysms that usually look like a bulging on the arterial walls with either saccular or fusiform shape. These pathologies are formed due to non-physiological remodelling of the vessel walls, occurring when the excessive stress is exerted on them over a long period of time. Untreated aneurysm can rupture leading to internal bleeding, haemorrhagic stroke, permanent brain damage and, consequently, permanent disability, coma or even death.

The most dangerous aneurysms are located at the aorta and in the region of the brain (cerebral, intracranial aneurysms, IAs). It is reported that 25-50% of IAs rupture cases end up with the patient death. Around 33% of survivors suffer from permanent brain damage that manifests itself with severe neurological and cognitive deficits [9]. When it comes to the prevalence of IAs among human population, one can find varied information: 5.0-8.0% [17], 1.5-8.0% [8], 0.4-3.6% (cadaveric studies) and 3.7-6.0% (angiographic examinations) [12]. Early detection of the aneurysm presence and a choice of the most suitable method of its treatment are of an utmost importance in clinical practice. When it comes to a treatment of cerebral aneurysms, currently there are two main possibilities, i.e. surgical procedures and endovascular methods. In both methods we can distinguish further varied sub-techniques that present some advantages and disadvantages when compared to the others.

Focusing on the endovascular methods, the most commonly applied techniques include coiling (together with its slight modifications, i.e. stent-assisted coiling or balloon-assisted coiling), Flow Diverter (FD) stents and Intrasaccular Flow Disruptors. FDs are made of elastic, circular wires and they are significantly less porous than the standard stents. Due to high mesh density, FDs reduce an inflow to the aneurysm sac, and thus they may lead to a formation of an environment suitable for intrasaccular thrombosis (regions of low velocity and elevated viscosity). Moreover, high density of very small pores can be regarded as a scaffold for the endothelium that, over time, can cover the small pores and serve as a further separation barrier that limits the inflow/outflow to the aneurysm.

The choice of the FD to be implanted for the given patient is made by a physician based on her/his experience. This can be additionally supported by computational fluid dynamics (CFD) tools, i.e. through thorough qualitative and quantitative analysis of the numerical data obtained thanks to the numerical simulations of the blood flow. By comparing the hemodynamic environment in pre- and post-treatment geometries, scientists can gather interesting data regarding e.g. flow velocity and its vorticity as well as stresses exerted on the aneurysms walls. This has been already proved for simple and idealized geometries of the aneurysms. For instance, Sanches et al. [27] investigated differences in flow haemodynamics resulting from virtual implantation of regular stent and FD into a simple model of the artery (straight vessel of a constant diameter) and ideally spherical aneurysm. They noted larger reduction of the wall shear stress (WSS) as well as larger reduction in intrasaccular flow velocity for the FD case study, which confirms that this type of stents might be better at promoting intrasaccular thrombosis [27]. In 2024, Kim et al. [15] analysed hemodynamic changes resulting from the size of FD and parent artery. They prepared four physical and corresponding four virtual models of the idealized arteries with the spherical aneurysm. Afterwards, these researchers implanted real and virtual FDs into the geometries and analysed the flow experimentally as well as numerically. It turned out that a shift from oversized to undersized FD resulted in the reduction of velocity and energy loss. Thus, they confirmed that selection of the proper size of the FD is crucial to obtain a desired flow diversion effect.

Janiga et al. [9] presented an automatic CFD-based FD optimization principle for patient-specific IAs and they investigated 7 different configurations of automatically deployed FDs. This research group concluded that presence of each stent resulted in a reduction of intrasaccular velocity as well as WSS exerted on the walls. Blood flow reduction differences varied depending on the positioning of the local stent compression [9]. Other research groups have also proposed numerical methods of the virtual stent deployment to mimic the real behaviour (expansion and fitting) of the stents that can be followed by CFD analyses [20, 5].

The major shortcoming of in-silico analyses is the required computational cost – the larger the numerical mesh, the longer the calculation time and the larger the computational demand (such as RAM or available disk space). The explicit presence of the FD requires very dense discretization around the wirebraid, which, consequently, leads to generation of enormous meshes (consisting of dozens/hundreds of millions of elements) and huge computational demand. Therefore, some researchers try to substitute the presence of the stent by porous medium. This approach requires defining some parameters related to additional resistances, i.e. inertial and viscous ones, that are taken into account by the numerical solver that calculates an additional pressure drop. Despite being very promising technique, porous medium approach seems to be burdened with significant discrepancies of the estimated results. For instance, Augsburger et al. [4], who replaced FD structure with a homogenous porous medium governed by Darcy-Forccheimer formula, noted differences in velocity and WSS exceeding 20%, while discrepancies in shear rate and vorticity were approximately 31% and 47%, respectively. Kim et al. [13] used the Idelchik model two high-porosity stents as homogenous porous media. They proved that stent porosity has a significant influence on several hemodynamic parameters such as aneurysmal stasis and WSS [13].

Then, other scientists started to include the heterogeneity of the stent structure in their porous media and the results were characterized by lower errors than the results obtained with the standard homogeneous models. For example, Farsani et al [32] established an algorithm that determines which node of the numerical mesh intersects with the stent structure and then it maps an additional pressure drop at that region. Such an approach helped them in obtaining the solution that was in conformity with the data calculated for the explicit stent presence (difference in the inflow to the aneurysm equal to around 3.5%) [32]. Dazeo et al. [7] decided to compare varied approaches of modelling the FD as a porous medium: homogeneous model as presented in [4], homogeneous model using modified Idelchik technique [25], homogeneous model with coefficients based on statistical properties [21] and heterogenous variant of the latter two techniques. This extensive research, conducted for 14 patient-specific geometries, showed that each method is burdened with non-negligible errors, hence, despite significant reduction in computation time, the results have to be thoroughly checked and validated. Abdehkakha et al. [1] presented their new approach of modelling the stent as inhomogeneous porous medium that behaves as a thin screen in which the additional pressure drop is calculated cell-by-cell. This allowed them to obtain the results characterized by a very good agreement with the data obtained for the explicit device (e.g. differences in intrasaccular velocity not exceeding 4%, in shear rate around 1%, while in turnover time 6% in average). Despite obtaining reliable results in definitely shorter time (approximately 5 times faster), the study was based on stead-state assumptions, so their approach has not been validated for rapidly changing boundary conditions and for non-Newtonian blood flows [1]. Nonetheless, the methods presented by Abdehkakha et al. [1] seem to be very promising.

Apart from porous medium substitution, the FD stent can be modelled with another approach called Immersed Solid Method (ISM). This requires generating two separate meshes – one for the fluid domain and the other for the solid domain (an obstacle in the flow). Then, mesh of the solid is projected onto the fluid mesh and fluid velocity is set as 0 m/s at the overlapping nodes. This approach has not been widely used for mimicking the stent presence – there is hardly any publication on this matter. However, Lohner et al. [19] performed a comparison between body-fitted, embedded and immersed solid solutions for the flow around two obstacles, i.e. a sphere and a stent. They achieved a very high correlation of the results obtained with explicit technique and ISM which suggests that this method can be treated as a reliable one. Raschi et al. [25] compared the results of the flow obtained with ISM method and porous modelling – they noted a high agreement between both datasets and they emphasized that porous medium approach reduces the computation time in a ten-fold manner. However, they had to perform initial fine-tuning of the parameters defining the porous medium – mainly coefficients of the quadratic curve representing a dependence of the pressure drop on velocity [25]. It is worth pointing out that ISM can be regarded as a compromise between explicit approach and porous medium modelling.

Based on all the aforementioned information, the main objective of this research was to analyse an influence of the FD stent porosity on the intrasaccular flow haemodynamics utilizing CFD with ISM approach. For that purpose, we conducted in-silico studies of blood flows in patient-specific model of the cerebral vasculature, before and after the virtual implantation of the selected FDs. We have chosen stents with the following nominal diameters: 4.5, 5.0, 5.5 and 6.0 mm. During steady state and pulsatile flow simulations we analysed numerous hemodynamic properties, such as velocity, normal and tangent stress, intrasaccular stasis and blood viscosity.

## 2. Materials and methods

Carrying out steady state and transient numerical simulations of the blood flow, utilizing the ISM, required fulfilling numerous steps. The most important information regarding the major steps is provided in this section

### 2.1. Patient-specific geometry

After importing the biomedical imaging data obtained with computed tomography angiography (CTA) into the custom-developed AMR software (Lodz University of Technology, Poland), the authors applied an algorithm that artificially enhances the dataset resolution, making the segmentation procedures easier. Then, 3D region growing algorithm was used to separate arteries filled with a contrast agent from the surrounding tissues. Unfortunately, the prepared 3D binary mask with marked region of interest (ROI) had numerous shortcomings, i.e. improperly added or lacking voxels, and thus additional manual segmentation procedures were required. Once the binary mask was prepared, one had to extract the surface model of the arterial lumen and then apply smoothing operation. Afterwards, each efferent and afferent vessel had to be clipped in its proximal or distal end to obtain perpendicularly aligned openings resembling inlet and outlet surfaces. To get rid of any unwanted artifacts on the prepared surface object (such as spikes, non-manifold faces or self-intersecting edges), it was saved as stereolithography (STL) file and subjected to polyhedral meshing using ANSYS Fluent (ANSYS Inc., USA). After generation of the polyhedral mesh with proper local sizing of the elements, the wall was saved as STL once again and sent to ANSYS SpaceClaim (ANSYS Inc., USA). Within that software, STL file was converted into the standard 3D surface object and was exported in the Parasolid (.x_t) format that allows the given file to be imported into majority of computer-aided design (CAD) programs. The last step was to convert the surface model into a typical volumetric one using SolidWorks software (Dessault Systemes S.A., France). Such a transition allows for a faster and simpler processing of the 3D geometry, required during further steps. It is worth emphasizing that for the numerical simulations we have chosen just a fragment of the entire 3D model. Since this particular patient did not have complete circle of Willis, i.e. lack of both posterior communicating arteries and anterior communicating artery, we decided to use only the arteries that were directly and indirectly connected with the parent artery changed with the aneurysm. The final model is presented in Fig. 1.

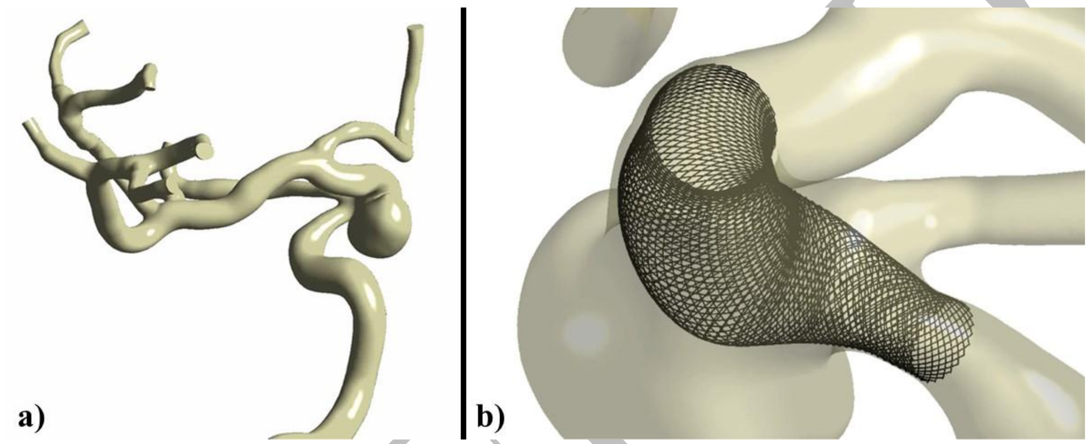


Fig. 1. Virtual models used in this research: a) fragment of the patient-specific arterial tree network; b) FD stent (Ø4.5 mm) implanted in the parent artery

### 2.2. Flow Diverter geometry

To retrieve the approximated geometrical characteristics of the stent topology, the authors had to develop a software that would calculate braiding angles of the stent wireframe after its fitting to the arterial walls and help in recreating the stent geometry inside SolidWorks program. After clipping the 3D model in a suitable manner (leaving just the parent artery with the aneurysm), one had to extract the parent artery centreline. For that purpose, the authors used Vascular Modelling Toolkit, i.e. VMTK software [3]. Then, once the centreline was loaded into the custom-developed software called MED-SPG (Lodz University of Technology, Poland), uniformly distributed points were projected along the centreline. Afterwards, the authors had to select points that would serve as the basis for the circular contour extraction – each contour had a diameter calculated by Voronoi principle (thanks to VMTK package) and represented maximum inscribed sphere at that particular point. If the maximum nominal diameter of the uncompressed stent was smaller than diameter of the parent artery, then the stent diameter was chosen for the final calculations. After selecting desired cross sections for the stent pathway and its circumference, MED-SPG calculated the average braiding angle, taking into account that nominal topological features of the stent (nominal diameter, nominal length and nominal braiding angle) had to locally change due to the stent deformation. Such deformation occurred in the areas where the FD had to compress itself to fit to the narrower part of the parent artery. The nominal diameters of the stents were as follows: 4.5, 5.0, 5.5, 6.0 mm, while the nominal braid angle was assumed to be constant and equal to 75°, as presented in the other study [18]. However, for each stent configuration, the resultant, final braiding angle varied due to the aforementioned changes in the stent topology. Once the circular cross sections and final braiding angle were prepared for each FD, MED-SPG allowed one to export specific macro files compatible with SolidWorks program.

Within SolidWorks, the authors had to import the generated macro thanks to which, after few additional complex steps (such as preparation of the stent "sleeve" and 48 helical construction surfaces rotated by the calculated braiding angle), pathways for every single wire of the FD were prepared. Then, for each pathway we applied a method of circular cross section lofting, where the diameter of the wire was set as 33 μm, according to the available specification. Finally, all volumetric models of the wires were saved as STEP files. The model of the stent Ø4.5 mm is depicted in Fig. 1.

### 2.3. Numerical domain

Our numerical simulations of the blood flow in post-treatment geometries were based on the ISM available in ANSYS CFX solver (ANSYS Inc., USA) – we had to map the vortices of the stent solid mesh onto the fluid domain mesh. Thus, to capture flow phenomena occurring in the vicinity of the stent wirebraid, the authors had to apply local condensation of the elements in the regions where the FD should be present. After performing mesh independence tests, it turned out that the element size of 11 μm, used in the Body of Influence, was the most optimal one. Each mesh was composed of tetrahedral elements and an inflation layer that was made of 8 sublayers with prismatic elements (generation scheme: smooth transition; growth rate: 1.15). The final numerical meshes were as follows: stent Ø4.5 mm – 43.2 million elements, stent Ø5.0 mm – 38.0 million elements, stent Ø5.5 mm – 34.3 million elements, stent Ø6.0 mm – 31.6 million elements.

The flow was assumed to be adiabatic and isothermal with turbulence model set as k-ω SST (Shear Stress Transport). Blood was treated as an incompressible fluid of constant density equal to 1060 kg/m$^3$, as in the other CFD studies [2, 23, 24]. Additionally, it was characterized by non-Newtonian shear-thinning behaviour – the viscosity was governed by the modified power law formula – see Eq. 1. Such a rheological model has been already proposed and used in numerous other researches [10, 11, 26, 30, 31].

$$\begin{cases} \boldsymbol{\eta = 0.55471\ \mathrm{Pa \cdot s}} & \text{for } \dot{\gamma} \leq 0.001 \\ \boldsymbol{\eta = \eta_0 \cdot (\dot{\gamma})^{n-1}} & \text{for } 0.001 \leq \dot{\gamma} < 327 \\ \boldsymbol{\eta = 0.00345\ \mathrm{Pa \cdot s}} & \text{for } \dot{\gamma} \geq 327 \end{cases} \quad \text{Eq. (1)}$$

where: $\eta_0 = 0.035$ kg·m$^{-1}$·s$^{-1.4}$; $n = 0.6$

When it comes to the boundary conditions, one has to discuss them separately for steady state and transient simulations. For the pulsatile boundary conditions, time-dependent inflow was assumed at the inlet cross section and time-dependent pressure values were set at all the outlet surfaces (the same for every single outlet cross section). The velocity characteristics were estimated in such a way that the inflow through the internal carotid artery (ICA) was physiological. According to the literature, approximately 5.3% of the cardiac output is delivered by the ICA throughout an entire cardiac cycle [16]. Taking into account this information and knowing an area of the ICA inlet surface, we calculated proper amplitude of velocity so that time-averaged value of volume flow rate corresponded to 4.24 cm$^3$ per single cardiac cycle (5.3% of 80 cm$^3$). Moreover, to preserve non-uniform velocity distribution at the inlet cross section, Prandtl profile was applied – see Eq. 2. When it comes to steady state simulations, we assumed constant pressure equal to 11.5 kPa at the outlet cross sections and constant value of velocity equal to 31 cm/s (maximum velocity in Prandtl formula) which corresponded to the aforementioned, cycle-averaged physiological volume flow rate.

$$V_p = V_{max} \cdot \left(1 - \frac{r}{R_{max}}\right)^{1/7} \quad \text{Eq. (2)}$$

where: $V_{max}$ = velocity amplitude, $R_{max}$ = maximum radius of the parent artery.

Steady state simulations were treated as fully solved once the values of the residual criteria dropped below $10^{-6}$ or once the maximum number of iterations (500) was reached. In most cases, the simulations converged after around 420 iterations. Transient analyses were carried out for 4 seconds (5 full cardiac cycles) with a timestep equal to 0.008 s. Steady state simulations were carried out for every single case study, while transient ones for the reference geometry (no stent), stent Ø4.5 mm and stent Ø6.0 mm. It was decided to limit the number of pulsatile simulations due to the fact that a single case study occupied around 250 GB of disk space and took approximately 7 days to be calculated. Basic parameters of the computing workstation: AMD Ryzen Threadripper processor with 32 cores and 4.0 GHz CPU clock speed.

## 3. Results

During this research, we focused on analysing several hemodynamic indicators that might suggest whether the aneurysm has a lower possibility of rupture. This includes stress acting on the aneurysm walls (both normal and tangent), areas of intrasaccular stagnant blood and regions with elevated viscosity of blood. Moreover, we investigated differences in the global blood flow distribution resulting from the FDs presence and their varied porosity.

### 3.1. Resolution of ISM

Before the data related to securing the aneurysm is presented, it was decided to show the potential of ISM as a substitute for traditional approach of simulating the FD explicitly. For that purpose, the authors modelled the stent explicitly, however, its structure was limited only to the neck of the aneurysm (to reduce the number of elements in the domain). Similarly, the same stent topology was used to generate the next mesh using the ISM. After performing steady state and transient simulations, it turned out that the vast majority of analysed parameters are in good agreement with one another – see Table 1. After positive validation of ISM, the authors investigated velocity distribution at the control surface in the target simulation (see Fig. 2) and observed whether the ISM reliably captured local changes in flow haemodynamics.

Table 1: Comparison of the results obtained with varied methods of FD modelling

| | No stent | Explicit stent | ISM stent | ISM vs explicit |
|---|---|---|---|---|
| Flow rate at *Control Plane #1* [$cm^3/s$] | **0.586** | **0.538** (-8.2%) | **0.541** (-7.7%) | 0.6% |
| Flow rate at *Control Plane #2* [$cm^3/s$] | **3.089** | **3.100** (0.4%) | **3.105** (0.5%) | 0.2% |
| Area-averaged pressure [Pa] | **10229** | **10249** (0.2%) | **10254** (0.2%) | 0.0% |
| Maximum pressure [Pa] | **10267** | **10260** (-0.1%) | **10261** (-0.1%) | 0.0% |
| Area-averaged WSS [Pa] | **3.34** | **1.20** (-64.1%) | **0.88** (-73.7%) | -26.7% |
| Maximum WSS [Pa] | **37.89** | **14.26** (-62.4%) | **15.14** (-60.0%) | 6.2% |
| Volume-averaged viscosity [mPa·s] | **4.39** | **5.85** (33.3%) | **6.04** (37.6%) | 3.2% |

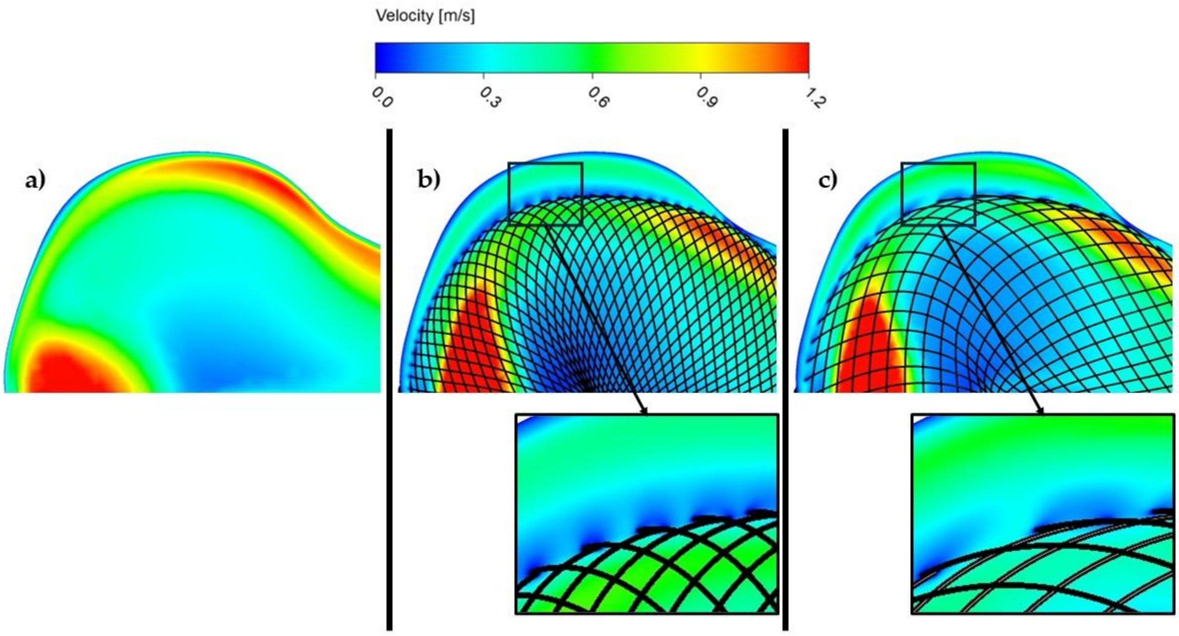


Fig. 2. Blood velocity distribution at a random control surface:
a) reference geometry (no stent); b) stent Ø4.5 mm; c) stent Ø6.0 mm

Despite not having modelled the FD explicitly (no physical presence of the stent), the influence of the wirebraid in ISM is clearly visible. One can note that inside each stent pore there is a local acceleration of blood. Each stent configuration partly inhibits the flow through its solid structure, what confirms that ISM captures the most important phenomena of the flow haemodynamics using the "immersed solid" body.

It is worth emphasizing that ISM allowed for a drastic decrease in computational time due to significant reduction of the elements forming the mesh. The meshes were composed of approximately 41.0 and 8.9 million elements for the stent modelled with explicit approach and ISM, respectively. The corresponding simulation time was equal to 39 hours for explicit stent and 5.5 hours for ISM, so we noted a seven-fold decrease in the computational time demand. We would like to remind that the abovementioned validation was performed for the stent limited only to the neck of the aneurysm. If we tried to model an entire FD explicitly, we would obtain meshes composed of tremendous number of elements. Based on our experience with ISM, this technique generates circa 4.5 times smaller meshes than standard explicit approach. Since our ISM meshes for the entire FD are composed of approximately 40 million elements, we could assume that the corresponding explicit mesh would comprise around 180 million elements. For such case study, the computational time required for a single simulation to converge would be measured in weeks rather than days.

### 3.2. Blood flow distribution

Since it was proven that blood flow is partially blocked by the FD stent wirebraid, it was decided to analyse how the stent porosity influences blood flow distribution across the entire 3D domain. It is worth pointing out that differences in porosities of the FDs result only from the differences in the stent elongation (due to varied nominal diameters). The major emphasis was put on the ophthalmic artery since this vessel was partially covered by the stent struts. Such an analysis could help in determining whether presence of the stent can block an inflow to some arteries which, in turn, could lead to ischemic events. Table 2 outlines the numerical results of blood flow distribution obtained during steady state and transient simulations.

Table 2: Volume flow rate at every outlet surface in the 3D domain

| | | no stent | stent Ø4.5 | stent Ø5.0 | stent Ø5.5 | stent Ø6.0 |
|---|---|---|---|---|---|---|
| Steady state conditions volume flow rate [$cm^3/s$] | MCA #1 | **0.828** | **0.812** (-1.9%) | **0.809** (-2.3%) | **0.812** (-1.9%) | **0.812** (-1.9%) |
| | MCA #2 | **0.311** | **0.288** (-7.4%) | **0.288** (-7.4%) | **0.289** (-7.1%) | **0.291** (-6.4%) |
| | MCA #3 | **0.391** | **0.359** (-8.2%) | **0.363** (-7.2%) | **0.363** (-7.2%) | **0.366** (-6.4%) |
| | MCA #4 | **0.604** | **0.606** (0.3%) | **0.606** (0.3%) | **0.602** (-0.3%) | **0.603** (-0.2%) |
| | MCA #5 | **0.796** | **0.814** (2.3%) | **0.812** (2.0%) | **0.811** (1.9%) | **0.809** (1.6%) |
| | MCA #6 | **0.557** | **0.559** (0.4%) | **0.559** (0.4%) | **0.558** (0.2%) | **0.559** (0.4%) |
| | Ophthalmic | **1.092** | **1.149** (5.2%) | **1.150** (5.3%) | **1.150** (5.3%) | **1.145** (4.9%) |
| | ACA #1 | **0.721** | **0.712** (-1.2%) | **0.712** (-1.2%) | **0.713** (-1.1%) | **0.714** (-1.0%) |
| Blood supply during a single cardiac cycle [$cm^3$] | MCA #1 | **0.664** | **0.640** (-3.6%) | - | - | **0.642** (-3.3%) |
| | MCA #2 | **0.253** | **0.228** (-9.9%) | - | - | **0.229** (-9.5%) |
| | MCA #3 | **0.315** | **0.284** (-9.8%) | - | - | **0.288** (-8.6%) |
| | MCA #4 | **0.494** | **0.488** (-1.2%) | - | - | **0.485** (-1.8%) |
| | MCA #5 | **0.647** | **0.650** (0.5%) | - | - | **0.648** (0.2%) |
| | MCA #6 | **0.458** | **0.450** (-1.7%) | - | - | **0.450** (-1.7%) |
| | Ophthalmic | **0.828** | **0.925** (11.7%) | - | - | **0.919** (11.0%) |
| | ACA #1 | **0.582** | **0.572** (-1.7%) | - | - | **0.572** (-1.7%) |

MCA – middle cerebral artery; ACA – anterior cerebral artery

While analysing the data presented in Table 2, one can observe that despite being partially covered by the FD wirebraid, there was an increase in the inflow to the ophthalmic artery in all analysed case studies – on average, approximately 5.3% for steady state and 11.4% for transient ones. Non-negligible differences in blood supply to some other arteries could be noted as well, e.g. around 7% reduction for MCA #2 and MCA #3 segments in steady state simulations and around 9-10% reduction for the same vessels, but under pulsatile conditions. This suggests that stent presence influences blood flow directioning globally. When comparing the results obtained just for the cases with FD implanted, majority of the results show insignificant differences. As expected, the largest discrepancies could be observed for the marginal porosities of the FD, i.e. for the stent Ø4.5 mm and stent Ø6.0 mm. The highest difference was equal to 1.8% for the MCA #3 branch in steady state case studies and 1.2% for the MCA #3 in transient ones.

### 3.3. Stress acting on the aneurysm wall

The factor that is usually associated with the aneurysm rupture is excessive stress (pressure and WSS) acting on the vessel walls. If the aneurysm is subjected to elevated pressure and WSS, the mechanical properties of its walls start to degrade over time. Consequently, the wall gets weaker and it might eventually rupture leading to internal haemorrhage. Therefore, for each analysed case study we investigated these parameters. Figure 3 outlines a qualitative comparison of pressure distribution just at the aneurysm wall for the reference and the most dense stent, i.e. of nominal diameter equal to 4.5 mm.

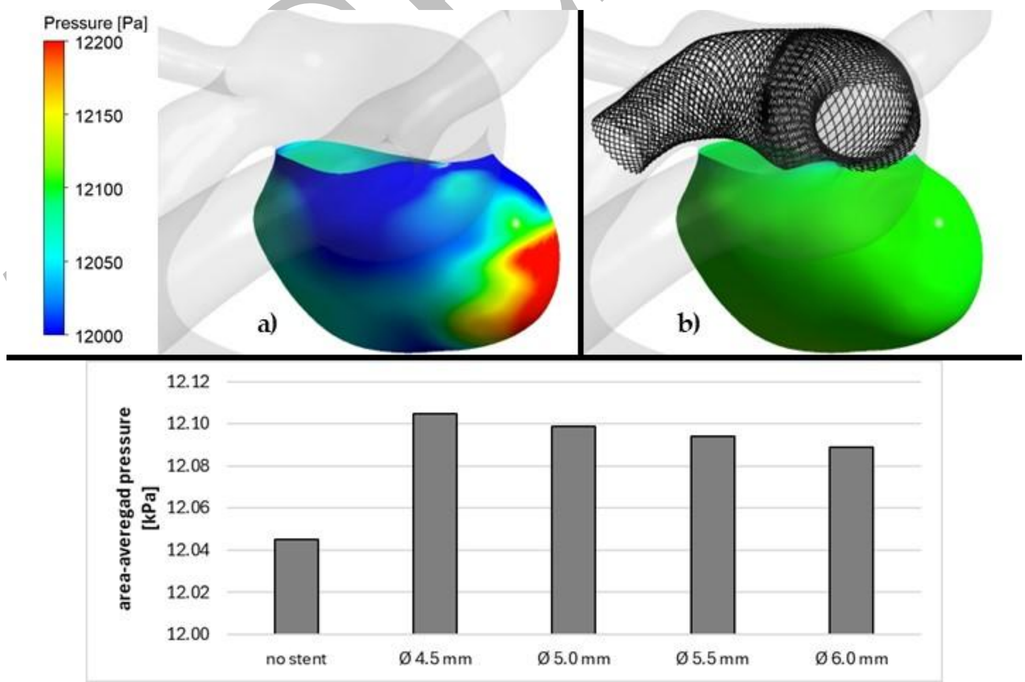


Fig. 3. Pressure distribution and its magnitude: a) reference case study; b) stent Ø4.5 mm; c) values calculated for each steady state case study

The first observation was that presence of the FD stent contributed to the creation of more uniform pressure distribution at the aneurysm wall. It is clearly visible in Fig. 3 – in the reference case study, aneurysm is subjected to a broad range of pressure (and thus there is a local concentration of elevated stress), whereas in the post-treatment geometry hardly any changes in pressure amplitude can be noted. The authors assumed that the denser the stent, the higher the degree of the flow inhibition, and consequently lower the inflow to the aneurysm sac, which, in turn, might have lowered stress values. This assumption was proved to be correct while analysing maximum pressure, area-averaged WSS and maximum WSS exerted on the aneurysm walls – see Fig. 4. However, the opposite relation was observed for area-averaged pressure – the more porous the stent (the larger its nominal diameter), the lower the area-averaged pressure. For instance, the maximum pressure value was equal to circa 12.25 kPa for the reference geometry and it dropped to circa 2.15 kPa for the most porous stent (Ø6.0 mm) and to 12.13 kPa for the least porous FD (Ø4.5 mm). When it comes to area-averaged pressure, we noted an increase from ca 12.05 kPa (for the reference) to 12.09 kPa for the most porous stent and to 12.10 kPa for the densest stent. It suggests that an increase of the stent density flattens the pressure range span over the aneurysm walls – it lowers the maximum pressure and increases area-averaged one. Additionally, the more dense the stent, the larger the reduction of intrasaccular flow velocity, which, in turn, lowers the WSS (due to lower gradients of velocity near the wall) and increases the static pressure, which is in agreement with principles of fluid mechanics.

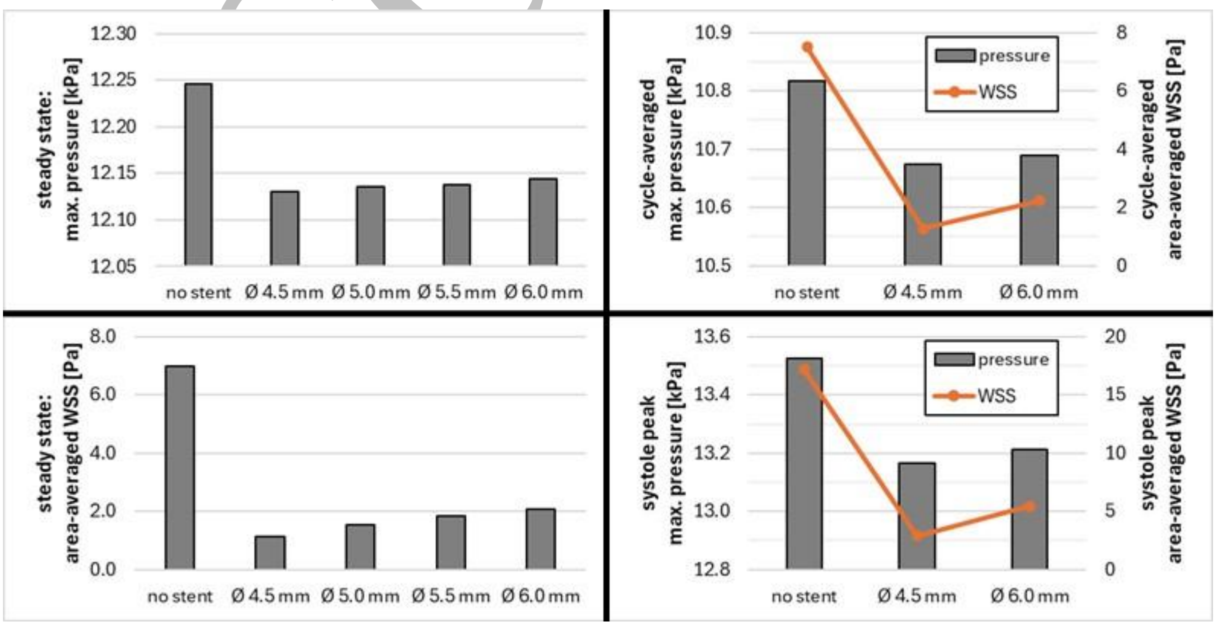


Fig. 4. Stress acting on the aneurysm wall – results for steady state and pulsatile flow conditions

### 3.4. Environment promoting intrasaccular thrombosis

Apart from reducing the stresses acting on the aneurysm wall, there is another aspect that might prevent the aneurysm from rupture – creation of an additional support for the aneurysm wall. Once the blood is trapped inside the aneurysm, it starts to flow with very low velocity and might be "trapped" in a recirculation zone. Then, its viscosity starts to increase and after some time thrombogenic process might begin. The formed blood clot can stick to the aneurysm wall and can serve as an additional mechanical support. Bearing that in mind, the authors analysed regions of stagnant blood and intrasaccular blood viscosity for each analysed case study. Additionally, we introduced two parameters: *relative volume of stagnant blood* (RVSB), i.e. region where blood velocity drops below 0.01 m/s, and *relative volume of viscous blood* (RVVB) which takes into account blood with viscosity at least two times higher than the standard reference value, i.e. equal to or greater than 6.9 mPa·s. Table 3 outlines the values of both these parameters for steady state case studies, Fig. 5 shows a graphical comparison of the RVVB parameter, while Fig. 6 presents viscosity values obtained during transient analyses.

Table 3: Relative volume of intrasaccular stagnant and viscous blood: steady state results

| | ref. (no stent) | stent Ø4.5 | stent Ø5.0 | stent Ø5.5 | stent Ø6.0 |
|---|---|---|---|---|---|
| RVSB | **0.00%** | **2.29%** | **1.02%** | **0.48%** | **0.37%** |
| RVVB | **0.37%** | **20.11%** | **13.41%** | **6.35%** | **4.81%** |

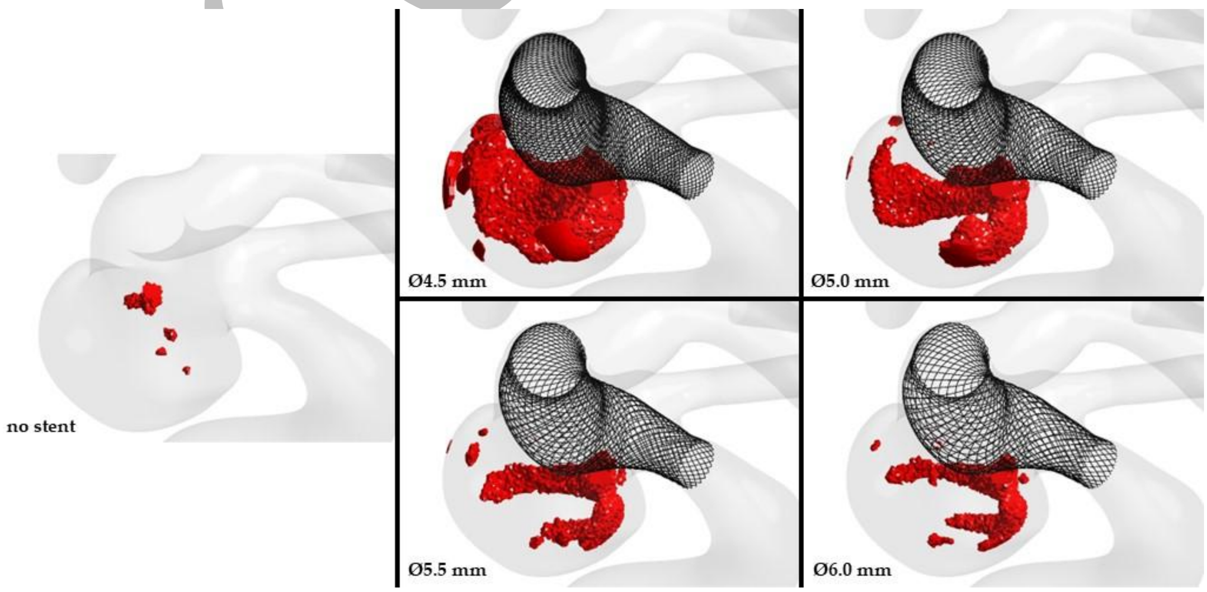


Fig. 5. Qualitative comparison of RVVB parameter inside the aneurysm dome

As can be noted from Table 3 and Fig. 5, the denser the stent, the larger the RVSB parameter (which means that the volume occupied by low-velocity blood is larger). In the stent Ø4.5 mm, RVSB was equal to 2.29%, while for the most porous stent, Ø6.0 mm, 0.37%. Similar observation could be noted for RVVB parameter – the more porous the stent, the lower the volume of regions characterized by elevated viscosity, i.e. 4.81% for the stent Ø6.0 mm and 20.11% for the stent Ø4.5 mm. Therefore, it seems that the more packed the FD, the better.

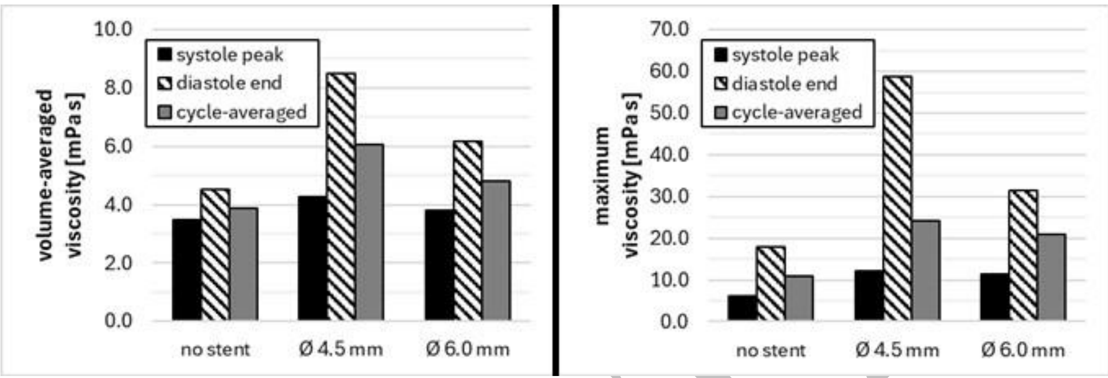


Fig. 6. Comparison of blood viscosity values for the pulsatile flow simulations

Once we analysed the transient results, we confirmed the observations done for the steady state case studies. We noted an increase in RVSB, RVVB and viscosity values with an increase of the stent density. For instance, the volume-averaged viscosity measured at the diastole end (when velocity is the lowest and consequently viscosity is the largest) was equal to 8.5 mPa·s for the stent Ø4.5 mm and slightly over 6.0 mPa·s for the stent Ø6.0 mm. During the systole peak this difference was not so significant, i.e. approximately 4.3 vs 3.8 mPa·s. When it comes to the maximum intrasaccular viscosity, we noted its two-fold increase during late diastole – almost 60 mPa·s for the stent with 4.5 mm diameter and slightly over 30 mPa·s for the stent Ø6.0 mm. The difference between cycle-averaged results was not so exceptional – approximately 3.5 mPa·s (24.16 mPa·s for Ø4.5 stent and 20.81 mPa·s for Ø6.0 stent).

### 3.5. Blood washout analysis

The last parameter we investigated was a relative volume of “old blood” that remained in the aneurysm sac after each cardiac cycle – see Table 4 and Fig. 7. This could help in determining whether some portion of blood is trapped in the recirculation zone, is not washed out and consequently might have high affinity to initiate a possible thrombogenesis.

Table 4: Relative volume of intrasaccular "old blood" after each cardiac cycle

| time [s] | ref. (no stent) | stent Ø4.5 mm | stent Ø6.0 mm |
|---|---|---|---|
| 0.8 | 6.790% | 13.922% | 8.834% |
| 1.6 | 0.270% | 0.853% | 0.412% |
| 2.4 | 0.034% | 0.174% | 0.045% |
| 3.2 | 0.008% | 0.050% | 0.009% |
| 4.0 | 0.003% | 0.015% | 0.003% |

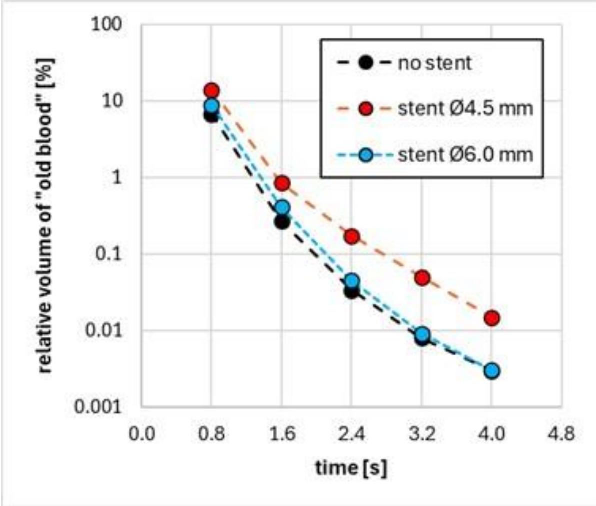


Fig. 7. Blood washout analysis as a plotted function for each transient case

As can be observed, the trendline of the blood washout function is similar in each analysed case study – the volume of "old blood" inside the aneurysm sac decreased rapidly, which means that despite presence of the stent, aneurysm was intensively washed out. After the second cardiac cycle the "old blood" occupied less than 1% of the aneurysm volume in each FD case study. Some differences between stents of varied porosities could be noted, especially for the initial cardiac cycles. As expected, the more porous stent (Ø6.0 mm), the lower the flow inhibition through the metal wirebraid structure and, consequently, the higher the washout phenomenon. After the first cardiac cycle, "old blood" was covering around 14.0% for the stent Ø4.5 mm, 8.8% for the other stent and 6.8% for the pre-treatment reference geometry. After the second cardiac cycle these values dropped to 0.85%, 0.41% and 0.27% respectively.

## 4. Discussion

This study was focused on an analysis of the FD stent porosity on the intrasaccular flow hemodynamics utilizing the numerical concept of ISM. Both steady state and transient analyses were performed, during which the authors could compare various parameters (velocity, stress, regions of blood stagnation and elevated viscosity) for pre- and post-treatment geometries.

Our analyses proved that the results obtained with the ISM are on par with the data obtained for the explicit presence of the stent and that ISM captures the most important phenomena of the flow haemodynamics around the wirebraid that is not physically present in the fluid domain. The flow rates and pressure values among case studies were almost identical and the highest differences were noted for the area-averaged WSS, maximum WSS and volume-averaged viscosity, i.e. 0.32 Pa, 1.12 Pa and 0.19 mPa·s, respectively. Thus, one can conclude that the differences can be regarded as negligible and that ISM technique is a reliable substitute for the explicit modelling. Our observations can be supported by a research of Lohner et al. who achieved a very high correlation of the results for a flow around the sphere and around the stent wirebraid [19] using the ISM and explicit approach. Another research group has also noted very good agreement of the results, although obtained with the ISM technique and porous medium modelling. However, they had to perform fine-tuning of the porous medium properties based on ISM results [25]. Similarly as in the other studies, we proved that presence of the stent (being an obstacle in the fluid domain) results in the reduction in intrasaccular flow velocity with a simultaneous decrease in WSS magnitude [15, 27]. Unfortunately, none of the available references present qualitative and/or quantitative data regarding the intrasaccular viscosity of blood, and thus, we cannot compare our results with data obtained by another scientific groups.

Some researches that present similar objectives (i.e. investigation of the stent porosity) can be found in the literature, however, they are usually limited to simplified, idealized models of the aneurysms and various patterns of the FD wirebraid [6, 22] or the stent is modelled just at the neck of the aneurysm [28]. Nonetheless, majority of the results from these studies are in conformity with our observations. For instance, with a decrease in the FD porosity there is a decrease in the intrasaccular flow velocity which confirms that the denser the FD wirebraid, the larger the flow inhibition. When it comes to the WSS analysis, we calculated its values at the wall of the aneurysm, whereas Tang et al. investigated these parameters just at the aneurysm neck [28], while the other research groups in an entire domain [6, 22]. Additionally, none scientific group mentioned whether their numerical meshes were composed of an inflation layer near the wall – lack of this local condensation of thin-layered elements might have a significant impact on the estimated magnitudes of stress. Nonetheless, our research indicates that the denser the stent (or less porous it is), the lower the WSS exerted onto the aneurysm walls, which is in agreement with the observations presented in the other papers [6, 22]. With a decrease of the stent porosity, Tang et al. observed a very slight increase in the WSS magnitudes at the proximal part of the aneurysm neck and simultaneously a slight decrease at the distal part [28]. Thus, it is impossible to compare our data with the results obtained by this research group. In the other studies, the differences in porosity of the stents derive from the assumed compaction of the stents and/or implantation of numerous stents simultaneously, e.g. two layers of the same stent [33] or double/triple layer followed by artificial compaction of the stent [14]. The results of these researches are in agreement with the observations taken during the following study – the less porous the stent (or the more layers of the same stent are covering the aneurysm neck), the lower the intrasaccular velocity and WSS exerted on the aneurysm walls. However, the research of Kim et al. was based on an idealized geometry of the aneurysm and simple straight channel [14], while the study of Zhang et al. was based on patient-specific model of a single artery and an idealized aneurysm [33]. In our case studies, the 3D model was patient-specific one and it was not limited to just a single branch. Nonetheless, a vast majority of the presented data are in a good conformity. Area-averaged and maximum WSS as well as maximum pressure exerted on the aneurysm wall tended to decrease with a decrease in stent porosity, as expected. Area-averaged pressure presented opposite behaviour – it increased with a decrease of the stent porosity which is in agreement with the results of Kim et al. [14], who observed a slight increase in the static pressure for the case study with two FDs implanted when compared to the case study with just one FD implanted. This behaviour might be related to the basics of fluid mechanics – with a decrease in velocity, the static pressure increases. Since the decrease of the stent porosity (or alternatively speaking – the increase of the stent density) reduces intrasaccular velocity, the static pressure exerted on the aneurysm wall should increase.

In all our case studies the ophthalmic artery was partially covered by the FD wirebraid and we expected a drop in the blood flow rate through that vessel, similarly as presented in the study of Tang et al. [28]. However, we observed an unexpected increase in blood supply to that artery for every single post-treatment case study. The possible reason behind this phenomenon might be the fact that the presence of the stent in the proximal part of the parent artery lead to a creation of the sharper jet flow in the artery centre that could be pointed towards the FD pores located at the inflow to the ophthalmic artery. Additionally, changes in global flow rates due to varied stent porosity seemed to be relatively low in our case studies, while in the study of Tang et al. they were quite notable [28]. The reason behind this difference might be related to the complexity of the analysed models – our patient-specific geometry consisted of numerous channels and bendings, whereas the model presented by Tang et al. was an idealized geometry with a single bending [28].

When it comes to an assessment whether blood could start clotting inside the aneurysm, researchers analyse some additional metrics, such as relative residence time (RRT). This parameter is based on oscillatory shear index (OSI) and time-averaged wall shear stress (TAWSS) [6, 22]. It is claimed that RRT defines the slow-motion of the fluids near the aneurysm wall and that it can be used to assess the flow inhibition resulting with post-stenting intrasaccular thrombosis. The lower its value, the higher affinity to promote blood clotting. In our opinion this concept is valid, however, when only the near-wall region is analysed – the results cannot be projected on the regions in the centre of the aneurysm or in the free flow regime. Therefore, in our research, we directly investigated regions with very low velocity and high viscosity. We noted that the denser the stent, the larger the volume occupied by low-velocity blood (blood stagnation regions) and blood with elevated viscosity. Furthermore, our transient analyses proved that if the aneurysm neck is covered by more densely packed stent wires, there is a larger flow inhibition and, consequently, the aneurysm "rinsing" is reduced. This could be concluded after analysing the blood washout phenomenon. In case of the aforementioned researches [6, 22], they observed an increase in RRT parameter with an increase of the stent porosity and thus the conclusion is the same – the more porous the stent, the lower the chances of intrasaccular thrombosis.

The results presented in this research show a significant potential of CFD tools in planning the endovascular procedures – they help in analysing different virtual post-treatment scenarios, i.e. changes in hemodynamic parameters including pressure, WSS, intrasaccular velocity, intrasaccular viscosity and regions of stagnant blood. CFD tools can predict whether the density of the given stent is high enough to block an inflow to the aneurysm sack, creating an environment suitable for intrasaccular thrombosis, and simultaneously low enough to sustain an inflow to partially covered arteries and/or perforators. With such tools, neurosurgeons could observe possible outcomes of implanting particular stent without exposing the patient to any harm. As a result, they could select more promising variant of the stent for the particular patient.

## 5. Conclusions

The most important conclusions that could be drawn from this research are as follows:

1. The ISM is sufficient to analyse an influence of the stent presence on blood flow haemodynamics, both for steady state and pulsatile conditions.
2. Stent presence affects the global blood flow distribution across entire 3D model, and thus, the geometry shall not be limited to just a single pathological artery.
3. Changes in the porosity of the FD stent resulting from different nominal diameters (varied elongation of the pores) have a varied influence on the flow inhibition through the wirebraid structure, depending on the region of analysis. For the aneurysm (i.e. when the stent separates a "closed "zone) the differences were noticeable – the larger the porosity, the worse the aneurysm separation from the circulation. However, for the regions when there is a pressure gradient between inner- and outer-side of the stent, e.g.

artery that is covered by the stent struts, these differences were negligible - influence of the stent was approximately identical in each post-treatment case study.

4. The denser the stent, the larger the reduction of stress (pressure and WSS) exerted onto the aneurysm wall. Therefore, the possibility of the aneurysm rupture might be lowered.
5. The less porous the stent, the more possible the creation of an environment that promotes blood clotting – lower intrasaccular velocity, larger regions of blood stagnation and larger the volume occupied by blood characterized by elevated viscosity.

## References


1. Abdehkakha A, Hammond AL, Patel TR, Siddiqui AH, Dargush GF, Meng H. Cerebral aneurysm flow diverter modelled as a thin inhomogeneous porous medium in hemodynamic simulations. Comput Biol Med [Internet]. 2021;139(June):104988.
2. Ahadi F, Biglari M, Azadi M, Bodaghi M. Computational fluid dynamics of coronary arteries with implanted stents: Effects of Newtonian and non-Newtonian blood flows. Eng Reports. 2024;6(6).
3. Antiga L, Piccinelli M, Botti L, Ene-Iordache B, Remuzzi A, Steinman DA. An image-based modelling framework for patient-specific computational haemodynamics. Med Biol Eng Comput. 2008;46(11):1097–112.
4. Augsburger L, Reymond P, Rufenacht DA, Stergiopulos N. Intracranial stents being modelled as a porous medium: Flow simulation in stented cerebral aneurysms. Ann Biomed Eng. 2011;39(2):850–63.
5. Bouillot P, Brina O, Ouared R, Yilmaz H, Farhat M, Erceg G, et al. Geometrical deployment for braided stent. Med Image Anal. 2016;30:85–94.
6. Catalán-Echeverría B, Kelly ME, Peeling L, Bergstrom D, Chen X, Malvè M. CFD-based comparison study of a new flow diverting stent and commercially-available ones for the treatment of cerebral aneurysms. Appl Sci. 2019;9(7).
7. Dazeo N, Dottori J, Boroni G, Narata AP, Larrabide I. Stenting as porous media in anatomically accurate geometries. A comparison of models and spatial heterogeneity. J Biomech. 2020;110.
8. Gasparotti R, Liserre R. Intracranial aneurysms. Eur Radiol. 2005;15(3):441–7.
9. Janiga G, Daróczy L, Berg P, Thévenin D, Skalej M, Beuing O. An automatic CFD-based flow diverter optimization principle for patient-specific intracranial aneurysms. J Biomech. 2015;48(14):3846–52.

10. Jodko D, Jeckowski M, Tyfa Z. Fluid structure interaction versus rigid-wall approach in the study of the symptomatic stenosed carotid artery: Importance of wall compliance and resilience of loose connective tissue. Int j numer method biomed eng. 2022;38(8):1–23.
11. Jodko D, Obidowski D, Reorowicz P, Jóźwik K. Numerical investigations of the unsteady blood flow in the end-to-side arteriovenous fistula for haemodialysis. Acta Bioeng Biomech. 2016;18(4):3–13.
12. Keedy A. An overview of intracranial aneurysms. McGill J Med. 2006;9(2):141–6.
13. Kim M, Taulbee DB, Tremmel M, Meng H. Comparison of two stents in modifying cerebral aneurysm haemodynamics. Ann Biomed Eng. 2009;36(5):726–41.
14. Kim S, Yang H, Hong I, Oh JH, Kim YB. Computational Study of Hemodynamic Changes Induced by Overlapping and Compacting of Stents and Flow Diverter in Cerebral Aneurysms. Front Neurol. 2021;12(August):1–9.
15. Kim S, Yang H, Oh JH, Kim YB. Quantitative analysis of hemodynamic changes induced by the discrepancy between the sizes of the flow diverter and parent artery. Sci Rep. 2024;14(1):1–8.
16. Lantz BM, Foerster JM, Link DP, Holcroft JW. Regional Distribution of Cardiac Output: Normal Values in Man Determine by Video Dilution Technique. Am J Roentgenol. 1981;137(5):903–7.
17. Lee KS, Zhang JJY, Nguyen V, Han J, Johnson JN, Kirollos R, et al. The evolution of intracranial aneurysm treatment techniques and future directions. Neurosurg Rev [Internet]. 2022;45(1):1–25.
18. Ley D, Mühl-Benninghaus R, Yilmaz U, Korner H, Cattaneo GFM, Mailander W, et al. The Derivo Embolization Device, a Second-Generation Flow Diverter for the Treatment of Intracranial Aneurysms , Evaluated in an Elastase-Induced Aneurysm Model. Clin Neuroradiol. 2017;27:335–43.
19. Lohner R, Appanaboyina S, Cebral JR. Comparison of body-fitted, embedded and immersed solutions of low Reynolds-number 3-D incompressible flows. Int J Numer Methods Fluids. 2008;57:13–30.
20. Ma D, Dargush GF, Natarajan SK, Levy EI, Siddiqui AH, Meng H. Computer modeling of deployment and mechanical expansion of neurovascular flow diverter in patient-specific intracranial aneurysms. J Biomech [Internet]. 2012;45(13):2256–63.
21. Morales HG, Bonnefous O. Modelling haemodynamics after flow diverter with a porous medium. 2014 IEEE 11th Int Symp Biomed Imaging, ISBI 2014. 2014;(3):1324–7.

22. Nada A, Hassan MA, Fakhr MA, El-Wakad MTI. Studying the effect of stent thickness and porosity on post-stent implantation haemodynamics. J Med Eng Technol [Internet]. 2021;45(5):408–16.
23. Nogourani ZS, Alizadeh A, Salman HM, J. Al-Musawi T, Pasha P, Waqas M, et al. Numerical investigation of the effect of changes in blood viscosity on parameters hemodynamic blood flow in the left coronary artery with consideration capturing fluid–solid interaction. Alexandria Eng J. 2023;77:369–81.
24. Panganiban RJ, Lictaoa RR, Mesia ML, Amorado JA, Cabrera H. Computational Fluid Dynamics (CFD) in Arteriovenous (AV) Graft Implantation Through End-to-Side Anastomosis with Varying Tube Diameters Across Different Vascular Access Locations for Dialysis Treatment. Med. 2024;60(10).
25. Raschi M, Mut F, Lohner R, Cebral JR. Strategy for modelling flow diverters in cerebral aneurysms as a porous medium. Int j numer method biomed eng. 2014;30:909–25.
26. Reorowicz P, Tyfa Z, Obidowski D, Wiśniewski K, Stefańczyk L, Jóźwik K, et al. Blood flow through the fusiform aneurysm treated with the Flow Diverter stent – Numerical investigations. Biocybern Biomed Eng. 2022;42(1):375–90.
27. Sanches AF, Shit S, Özpeynirci Y, Liebig T. CFD to Quantify Idealized Intra-Aneurysmal Blood Flow in Response to Regular and Flow Diverter Stent Treatment. Fluids. 2022;7(8).
28. Tang AY-S, Chan H-N, Tsang AC-O, Leung GK-K, Leung K-M, Yu AC-H, et al. The effects of stent porosity on the endovascular treatment of intracranial aneurysms located near a bifurcation. J Biomed Sci Eng. 2013;06(08):812–22.
29. Timmis A, Vardas P, Townsend N, Torbica A, Katus H, De Smedt D, et al. European Society of Cardiology: cardiovascular disease statistics 2021: Executive Summary. Eur Hear J - Qual Care Clin Outcomes. 2022;8(4):377–82.
30. Tyfa Z, Obidowski D, Reorowicz P, Stefańczyk L, Fortuniak J, Jóźwik K. Numerical simulations of the pulsatile blood flow in the different types of arterial fenestrations: Comparable analysis of multiple vascular geometries. Biocybern Biomed Eng. 2018;38(2):228–42.
31. Wiśniewski K, Tyfa Z, Reorowicz P, Brandel MG, Adel T, Obidowski D, et al. Numerical flow experiment for assessing predictors for cerebrovascular accidents in patients with PHACES syndrome. Sci Rep. 2024;14(1):1–16.
32. Yadollahi-Farsani H, Scougal E, Herrmann M, Wei W, Frakes D, Chong B. Numerical study of haemodynamics in brain aneurysms treated with flow diverter stents using porous medium theory. Comput Methods Biomech Biomed Engin [Internet]. 2019;22(11):961–71.

33. Zhang H, Li L, Miao F, Yu J, Zhou B, Pan Y. Computational fluid dynamics analysis of intracranial aneurysms treated with flow diverters: A case report. Neurochirurgie. 2022;68(2):235–8.

## Acknowledgements

This research was funded by National Centre for Research and Development (Poland) grant number LIDER14/0034/2023. The sponsor had no role in the design or conduct of this research. The article was co-financed from the state budget of Poland and awarded by the Minister of Science within the framework of the Excellent Science II Programme.